

# Intrinsic quark transverse momentum in the nucleon from lattice QCD

Ph. Hägler,<sup>1</sup> B.U. Musch,<sup>1</sup> J.W. Negele,<sup>2</sup> and A. Schäfer<sup>3</sup>

<sup>1</sup>*Institut für Theoretische Physik T39, Physik-Department der TU München, 85747 Garching, Germany\**

<sup>2</sup>*Center for Theoretical Physics, Massachusetts Institute of Technology, Cambridge, Massachusetts 02139, USA*

<sup>3</sup>*Institut für Theoretische Physik, Universität Regensburg, 93040 Regensburg, Germany*

(Dated: October 17, 2018)

A better understanding of transverse momentum ( $\mathbf{k}_\perp$ -) dependent quark distributions in a hadron is needed to interpret several experimentally observed large angular asymmetries and to clarify the fundamental role of gauge links in non-abelian gauge theories. Based on manifestly non-local gauge invariant quark operators we introduce process-independent  $\mathbf{k}_\perp$ -distributions and study their properties in lattice QCD. We find that the longitudinal and transverse momentum dependence approximately factorizes, in contrast to the behavior of generalized parton distributions. The resulting quark  $\mathbf{k}_\perp$ -probability densities for the nucleon show characteristic dipole deformations due to correlations between intrinsic  $\mathbf{k}_\perp$  and the quark or nucleon spin. Our lattice calculations are based on  $N_f=2+1$  mixed action propagators of the LHP collaboration.

*Introduction.*— Already 30 years ago, it has been noted that intrinsic transverse momentum,  $\mathbf{k}_\perp$ , of partons gives rise to azimuthal asymmetries in unpolarized semi-inclusive deep inelastic scattering (SIDIS), for example  $e^- + p \rightarrow e^- + \pi + X$ , nowadays known as the Cahn effect [1]. Since then, significant progress has been made in understanding intrinsic  $\mathbf{k}_\perp$  effects and their relation to the eikonal phases that quark fields acquire in hadron scattering processes due to initial and final state interactions [2]. The eikonal phases, given by gauge links (Wilson lines), turn out to be *process-dependent* and lead to, e.g., the Sivers and Collins asymmetries [3, 4] in polarized SIDIS, which have attracted a lot of attention and were already observed in experiments at HERMES, COMPASS and Jefferson Lab [5]. Theoretically, these can be described in the framework of QCD factorization using transverse momentum dependent parton distribution functions (tmdPDFs) [4, 6], an approach that goes beyond the usual collinear approximation and operator product expansion involving (moments of) PDFs. In addition to their phenomenological importance, tmdPDFs provide essential information about the internal structure of hadrons in the form of probability densities in the transverse momentum plane,  $\rho(x, \mathbf{k}_\perp)$ , as illustrated in Fig. 1 [7], where  $x$  is the longitudinal momentum fraction carried by the quark.

In this work, we introduce process-independent  $\mathbf{k}_\perp$ -distributions and calculate these in lattice QCD. We illustrate our results by presenting  $\mathbf{k}_\perp$ -densities of quarks in the nucleon, with a focus on possible correlations between  $\mathbf{k}_\perp$  and the transverse quark and nucleon spins, resulting in deformations from a spherically symmetric

distribution. It is interesting to compare this approach with generalized parton distributions (GPDs) in impact parameter ( $\mathbf{b}_\perp$ -) space [8], which allows one to study the *spatial* distribution of partons in hadrons in form of probability densities  $\rho(x, \mathbf{b}_\perp)$  [9]. Lattice QCD studies of the latter revealed characteristic non-spherical shapes of the pion and the nucleon in the case of transversely polarized quarks [10, 11]. We stress, however, that tmdPDFs and GPDs provide fundamentally different and complementary insight into hadron structure, since they are not related by Fourier transformation and  $\mathbf{k}_\perp$  and  $\mathbf{b}_\perp$  are not conjugate variables.

To introduce the different tmdPDFs, we first define the momentum-space correlators  $\Phi_\Gamma = \Phi_\Gamma(x, \mathbf{k}_\perp; P, S)$ ,

$$\begin{aligned} \Phi_\Gamma &= \int d(\bar{n} \cdot k) \int \frac{d^4 l}{2(2\pi)^4} e^{-ik \cdot l} \tilde{\Phi}_\Gamma(l; P, S) \\ &= \int d(\bar{n} \cdot k) \int \frac{d^4 l}{2(2\pi)^4} e^{-ik \cdot l} \langle P, S | \bar{q}(l) \Gamma \mathcal{U} q(0) | P, S \rangle \end{aligned} \quad (1)$$

with nucleon states  $|P, S\rangle$  depending on momentum and spin, and where the Wilson line  $\mathcal{U} = \mathcal{U}_{C(l,0)}$ , defined by a path ordered exponential, ensures gauge invariance of the non-local quark operator  $\bar{q}(l) \dots q(0)$ . For the vector (unpolarized),  $\Gamma_V^\mu = \gamma^\mu$ , axial-vector (polarized),  $\Gamma_A^\mu = \gamma^\mu \gamma_5$ , and tensor (quark helicity flip),  $\Gamma_T^{\mu\nu} = i\sigma^{\mu\nu} \gamma_5$ , cases, the correlators in Eq. 1 can be parametrized by the twist-2 tmdPDFs [12]:

$$\begin{aligned} n_\mu \Phi_V^\mu &= f_1 + \mathbf{S}_i \epsilon_{\perp ij} \mathbf{k}_j \frac{1}{m_N} f_{1T}^\perp \\ n_\mu \Phi_A^\mu &= \Lambda g_1 + \frac{\mathbf{k}_\perp \cdot \mathbf{S}_\perp}{m_N} g_{1T} \\ n_\mu \Phi_T^{\mu j} &= -\mathbf{S}_j h_1 - \frac{\epsilon_{\perp ji} \mathbf{k}_i}{m_N} h_1^\perp \\ &\quad - \frac{\Lambda \mathbf{k}_j}{m_N} h_{1L}^\perp - \frac{(2\mathbf{k}_j \mathbf{k}_i - \mathbf{k}_\perp^2 \delta_{ji}) \mathbf{S}_i}{2m_N^2} h_{1T}^\perp, \end{aligned} \quad (2)$$

where the distributions  $f, g, h$  depend on  $x$  and  $\mathbf{k}_\perp$  and  $\Lambda$  is the nucleon helicity. The light-cone vectors  $n$  and

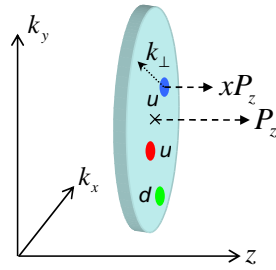


FIG. 1: Illustration of the transverse momentum distribution of quarks in the proton.

$\bar{n}$  in Eqs. 1,2 are chosen such that  $n \cdot \bar{n} = 1$ ,  $P = P^+ \bar{n} + m_N^2 / (2P^+) n$ , and the contraction with  $n_\mu$  in Eq. 2 projects on leading twist for large  $P^+$ . Formally [7], three of the tmdPDFs are directly related to the well-known unpolarized,  $f_1(x)$ , polarized,  $g_1(x)$ , and transversity,  $h_1(x)$ , PDFs by  $[f_1, g_1, h_1](x) = \int d^2 \mathbf{k}_\perp [f_1, g_1, h_1](x, \mathbf{k}_\perp)$ . Further (approximate) relations between tmdPDFs and GPDs have been established based on a dynamical mechanism [13], by analogy comparing  $\mathbf{k}_\perp$ - and  $\mathbf{b}_\perp$ -densities [9], and in the framework of quark models [14]. Such relations exist in particular for the Sivers,  $f_{1T}^\perp$ , and Boer-Mulders,  $h_1^\perp$ , functions, which are *naively* time-reversal odd. Remarkably, the tmdPDFs  $g_{1T}$  and  $h_{1L}^\perp$  cannot be directly related to any of the GPDs for reasons of time reversal symmetry, so that their appearance may be seen as *genuine* sign of intrinsic  $\mathbf{k}_\perp$  of quarks. In particular, they cannot be generated dynamically from coordinate ( $\mathbf{b}_\perp$ -) space densities by final state interactions. We emphasize that the definition of the correlator in Eq. 1 and therefore the tmdPDFs depends on the gauge link path  $\mathcal{C}(l, 0)$ . Apart from the precise form of  $\mathcal{C}(l, 0)$ , a further issue in the QCD factorization of SIDIS and Drell-Yan processes is the appearance of so-called rapidity divergences, which require regularization or subtraction and may be seen in analogy to the Bloch-Nordsieck theorem (see [15] and references therein). In the case of SIDIS, the path is generically given by  $\mathcal{C}(l, 0) = [l, l + \infty n, \infty n, 0]$ , which is not invariant under time reversal, and hence the appearance of the Sivers and Boer-Mulders functions. There exist two natural choices for process-independent  $\mathbf{k}_\perp$ -distributions, employing either a direct Wilson line  $\mathcal{C}(l, 0) = [l, 0]$ , or an average over all possible gauge links between 0 and  $l$ . We chose the first possibility for this pioneering study. Our results should not be directly compared to phenomenological studies of SIDIS [16] or the Drell-Yan process. In particular, the Sivers and Boer-Mulders functions vanish for direct Wilson lines. To describe the corresponding asymmetries, we will have to use specific gauge link structures, which is the subject of ongoing studies [17, 18]. Lattice QCD gives access to hadron matrix elements  $\tilde{\Phi}_\Gamma(l; P, S)$  (cf. Eq. 1), which can be parametrized by complex-valued invariant amplitudes  $\tilde{A}_i(l^2, l \cdot P)$ . The choice of a straight Wilson line, together with hermiticity, parity and time-reversal symmetry leaves us with 8 independent amplitudes:

$$\begin{aligned} \tilde{\Phi}_V^\mu &= 4P^\mu \tilde{A}_2 + 4im_N^2 l^\mu \tilde{A}_3, \\ \tilde{\Phi}_A^\mu &= -4m_N S^\mu \tilde{A}_6 - 4im_N P^\mu l \cdot S \tilde{A}_7 + 4m_N^3 l^\mu l \cdot S \tilde{A}_8 \\ \tilde{\Phi}_T^{\mu\nu} &= 4S^{[\mu} P^{\nu]} \tilde{A}_{9m} + 4im_N^2 S^{[\mu} l^{\nu]} \tilde{A}_{10} \\ &\quad - 2m_N^2 \left[ 2l \cdot S l^{[\mu} P^{\nu]} - l^2 S^{[\mu} P^{\nu]} \right] \tilde{A}_{11}, \end{aligned} \quad (3)$$

where  $[\mu\nu] = \mu\nu - \nu\mu$ . Detailed comparison with Eqs. 2 reveals that the tmdPDFs are given by certain Fourier-integrals of the amplitudes, where the Fourier conjugate variables are  $l \cdot P$  and  $x$ , and  $\mathbf{l}_\perp$  and  $\mathbf{k}_\perp$ . Such relations

exist between  $f_1 \leftrightarrow \tilde{A}_2$ ,  $g_1 \leftrightarrow \tilde{A}_{6,7}$ ,  $h_1 \leftrightarrow \tilde{A}_{9m}$ ,  $g_{1T} \leftrightarrow \tilde{A}_7$ ,  $h_{1L}^\perp \leftrightarrow \tilde{A}_{10,11}$ , and  $h_{1T}^\perp \leftrightarrow \tilde{A}_{11}$ , while  $\tilde{A}_{3,8}$  give only contributions to higher-twist tmdPDFs.

*Lattice QCD results.*— In our lattice study, we use a discretized, Euclidean version of the non-local operator  $\mathcal{O}_\Gamma(l) = \bar{q}(l) \Gamma \mathcal{U}_{[l,0]} q(0)$ . Limiting ourselves to purely spatial quark separations,  $l^0 = 0$ , the operator resides on a plane of equal Euclidean time. A product of connected link variables is used to represent the straight Wilson line  $\mathcal{U}_{[l,0]}$ . For oblique angles, we approximate a straight line by a step-like (zig-zag) path. According to the continuum analysis of Ref. [19], the renormalized operator can be written as  $O_\Gamma^{\text{ren}}(l) = \mathcal{Z}^{-1} \exp(-\delta m \sqrt{-l^2}) O_\Gamma(l)$ , involving two renormalization constants,  $\mathcal{Z}^{-1}$  and  $\delta m$ , the latter being associated with a potential power divergence of the Wilson line. The renormalization of Wilson lines in a cut-off regularized theory, e.g. on the lattice, and the appearance of power divergences of the form  $l/a$  has been studied extensively in the context of heavy quark effective theory, see, e.g., [20]. We utilize the fact that  $\delta m$  also appears in the renormalization of the static quark potential:  $V^{\text{ren}}(r) = V(r) + 2\delta m$ . At large  $r$ , the static quark potential is well approximated by the string potential  $V_{\text{string}}^{\text{ren}}(r) = \sigma r - \pi/12r + C^{\text{ren}}$ . To fix  $\delta m$  we follow Refs. [21] and match  $V^{\text{ren}}(r)$  to the string potential at  $r = 1.5r_0 \approx 0.7 \text{ fm}$ , setting  $C^{\text{ren}} = 0$ . Note that  $\mathbf{k}_\perp$ -distributions are sensitive to the renormalization condition implied by the choice of  $C^{\text{ren}}$ . In our numerical computations, we employ MILC gauge configurations [22] based on the AsqTad improved staggered quark action with two light and one heavier (strange) quark flavors. For our exploratory calculations, we have chosen an ensemble at a pion mass of  $\approx 500 \text{ MeV}$  and a lattice spacing of  $a = 0.124 \text{ fm}$ . From an analysis of  $V(r)$  from Wilson loops on the HYP smeared gauge configurations, we obtain  $a\delta m = -0.155(5)_{\text{stat}}$  [17, 18]. To determine the amplitudes  $\tilde{A}_i$ , we take advantage of the methods and techniques used in Ref. [23] for the calculation of GPDs. As in Ref. [23], we only include contributions from quark line connected diagrams. A major innovation in our analysis is that the lattice correlation (three-point) functions are evaluated for manifestly non-local operators  $\mathcal{O}_\Gamma(l)$ , hence requiring a parametrization according to Eq. 3. They are numerically evaluated using the CHROMA library [24] for domain wall quark propagators and sequential propagators previously calculated by the LHP collaboration, with the valence quark mass tuned to match the staggered sea quarks [23]. The sequential propagators are available for two lattice nucleon momenta  $\mathbf{P} = (0, 0, 0)$  and  $\mathbf{P} = (-1, 0, 0)$ , the latter corresponding to  $\approx 500 \text{ MeV}$  in physical units. We consistently use the nucleon mass of  $m_N = 1.291(23) \text{ GeV}$  obtained for this ensemble in the extraction of the amplitudes and tmdPDFs from Eqs. (2,3). All errors quoted are statistical (see Refs. [17, 18] for a more comprehensive treatment of uncertainties). Setting  $l^0 = 0$ , we are restricted to

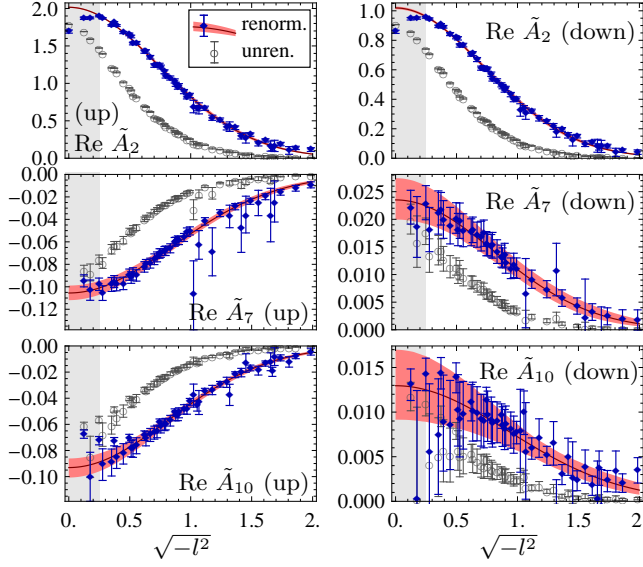


FIG. 2: Real parts of the amplitudes  $\tilde{A}_i(l^2, l \cdot P=0)$ , for  $m_\pi \approx 500$  MeV. The solid lines and error bands are Gaussian fits to the renormalized lattice data above  $\sqrt{-l^2}=0.25$  fm.

the region given by  $l^2 < 0$  and  $|l \cdot P| \leq \sqrt{-l^2}|P|$ . Since only finite hadron momenta  $P$  can be accessed on the lattice, this precludes us from evaluating the full  $x$ - and  $\mathbf{k}_\perp$ -dependence directly. An important result, demonstrated in detail by our lattice data in [17, 18] in the kinematic region accessible to us, is factorization of the  $x$  and  $\mathbf{k}_\perp$  ( $l \cdot P$  and  $l^2$ ) dependence to a good approximation. Factorization is a standard assumption for which we have now provided quantitative support, and for this reason we will focus in the following on the  $l^2$  dependence and present results for the lowest  $x$ -moments corresponding to  $l \cdot P = 0$ , e.g.,

$$f_1^{(0)}(\mathbf{k}_\perp) \equiv \int_{-1}^1 dx f_1(x, \mathbf{k}_\perp^2) = \int d^2 \mathbf{l}_\perp e^{i \mathbf{l}_\perp \cdot \mathbf{k}_\perp} 2 \tilde{A}_2(-l_\perp^2, 0).$$

We note that the  $x$ -integrated distributions of type  $f^{(0)}$  and  $h^{(0)}$  correspond to the difference, while distributions of type  $g^{(0)}$  correspond to the sum of quark- and antiquark distributions, respectively. Hermitian conjugation shows that  $\text{Im} \tilde{A}_i(l^2, l \cdot P=0)=0$ . Representative results for  $\text{Re} \tilde{A}_{2,7,10}(-l_\perp^2, 0)$  are displayed in Fig. 2. Similar results not shown in this work have been obtained for the amplitudes  $\tilde{A}_{6,9m,11}$ . We have parametrized our renormalized lattice data using a Gaussian ansatz  $2 \tilde{A}_i^{u,d}(-l_\perp^2, 0) = c_i^{u,d} \exp(-l_\perp^2/\sigma_i^{u,d})$ . Corresponding fits to the lattice data are represented by the error bands in Fig. 2. To avoid contamination by lattice cut-off effects at small  $l \lesssim a$ , we exclude data points for  $\sqrt{-l^2} \leq 0.25$  fm from the fit. The Gaussians smoothly bridge the excluded region at small  $l^2$ . Thus we do not resolve potential divergences of the amplitudes  $A_i(l^2, 0)$  in the continuum limit at  $l^2 \rightarrow 0$ . In that sense, the Gaussian parametrization effectively acts as a regularization pre-

	$c$	$2/\sigma$ (GeV)
$\tilde{A}_2^u$	$2.0159(86) = f_{1,u}^{(0,0)}$	$0.3741(72)$
$\tilde{A}_2^d$	$1.0192(90) = f_{1,d}^{(0,0)}$	$0.3839(78)$
$\tilde{A}_6^u$	$-0.920(35) = -g_{1,u}^{(0,0)}$	$0.311(11)$
$\tilde{A}_6^d$	$0.291(19) = -g_{1,d}^{(0,0)}$	$0.363(18)$
$\tilde{A}_{9m}^u$	$0.931(29) = h_{1,u}^{(0,0)}$	$0.3184(90)$
$\tilde{A}_{9m}^d$	$-0.254(16) = h_{1,d}^{(0,0)}$	$0.327(15)$
$\tilde{A}_7^u$	$-0.1055(66) = -g_{1T,u}^{(0,1)}$	$0.328(14)$
$\tilde{A}_7^d$	$0.0235(38) = -g_{1T,d}^{(0,1)}$	$0.346(36)$
$\tilde{A}_{10}^u$	$-0.0931(73) = h_{1L,u}^{\perp(0,1)}$	$0.340(14)$
$\tilde{A}_{10}^d$	$0.0130(40) = h_{1L,d}^{\perp(0,1)}$	$0.301(48)$

TABLE I: Parameters obtained from a fit of the amplitudes  $\tilde{A}_i(-l_\perp^2, 0)$  to Gaussian functions, for  $m_\pi \approx 500$  MeV.

scription at short distances  $l^2$ , which translates into a smooth cutoff of the resulting  $\mathbf{k}_\perp$ -distributions at large  $\mathbf{k}_\perp^2$ . Within this context, we define  $\mathbf{k}_\perp^2$ -moments

$$[f, g, h]^{(0,n)} = \int d^2 \mathbf{k}_\perp (\mathbf{k}_\perp^2/2m_N^2)^n [f, g, h]^{(0)}(\mathbf{k}_\perp^2).$$

Since  $f_1^{(0)}(\mathbf{k}_\perp^2)$  is the unpolarized density of quarks minus antiquarks, we can fix  $\mathcal{Z}$  by demanding that the total number of  $u$ - minus  $d$ -quarks in the proton is  $f_{1,u-d}^{(0,0)} = c_2^{u-d} = 1$ , giving  $\mathcal{Z}=1.056(14)$ . The Gaussian fit parameters are listed in Table I. Note that the width  $\sigma$  is very sensitive to our renormalization condition  $C^{\text{ren}} = 0$ . For  $\tilde{A}_{2,6,9m}$ , the inverse width  $2/\sigma = \langle \mathbf{k}_\perp^2 \rangle^{1/2}$  has an interpretation as the root mean square transverse momentum of the respective distribution  $f_1^{(0)}$ ,  $g_1^{(0)}$ ,  $h_1^{(0)}$ . The fact that  $g_{1,u-d}^{(0,0)} = 1.209(36)$  comes out close to the physical  $g_A = 1.2695(29)$  and agrees within errors with the direct calculation in [25] represents a remarkable validation of our approach. Interestingly, we find that  $g_{1T}^{(0,1)} \approx -h_{1L}^{\perp(0,1)}$ , which supports corresponding results obtained in quark model calculations [26]. The  $\mathbf{k}_\perp$ -densities of quarks in the nucleon for longitudinally ( $L$ ) and transversely polarized quarks ( $T$ ) can be obtained from  $\rho_L = \rho(x, \mathbf{k}_\perp; \lambda, \mathbf{S}_\perp) = n \cdot (\Phi_V + \lambda \Phi_A)/2$  and  $\rho_T = \rho(x, \mathbf{k}_\perp; \Lambda, \mathbf{s}_\perp) = (n \cdot \Phi_V - n_\mu s_j \Phi_T^{\mu j})/2$ , respectively, and appear in form of a multipole-expansion [9]

$$\begin{aligned} \rho_L &= \frac{1}{2} \left( f_1 + \lambda \Lambda g_1 + \left[ \frac{\mathbf{S}_j \epsilon_{ji} \mathbf{k}_i}{m_N} f_{1T}^\perp \right] + \lambda \frac{\mathbf{k}_\perp \cdot \mathbf{S}_\perp}{m_N} g_{1T} \right) \\ \rho_T &= \frac{1}{2} \left( f_1 + \mathbf{s}_\perp \cdot \mathbf{S}_\perp h_1 + \left[ \frac{\mathbf{s}_j \epsilon_{ji} \mathbf{k}_i}{m_N} h_1^\perp \right] \right. \\ &\quad \left. + \Lambda \frac{\mathbf{k}_\perp \cdot \mathbf{s}_\perp}{m_N} h_{1L}^\perp + \frac{\mathbf{s}_j (2\mathbf{k}_j \mathbf{k}_i - \mathbf{k}_\perp^2 \delta_{ji}) \mathbf{S}_i}{2m_N^2} h_{1T}^\perp \right), \quad (4) \end{aligned}$$

with monopole terms  $\propto f_1, g_1, h_1$ , dipole structures  $\propto f_{1T}, g_{1T}, h_{1L}^\perp, h_{1T}^\perp$ , and a quadrupole term  $\propto h_{1T}^\perp$ . The terms in square brackets proportional to the T-odd Sivers



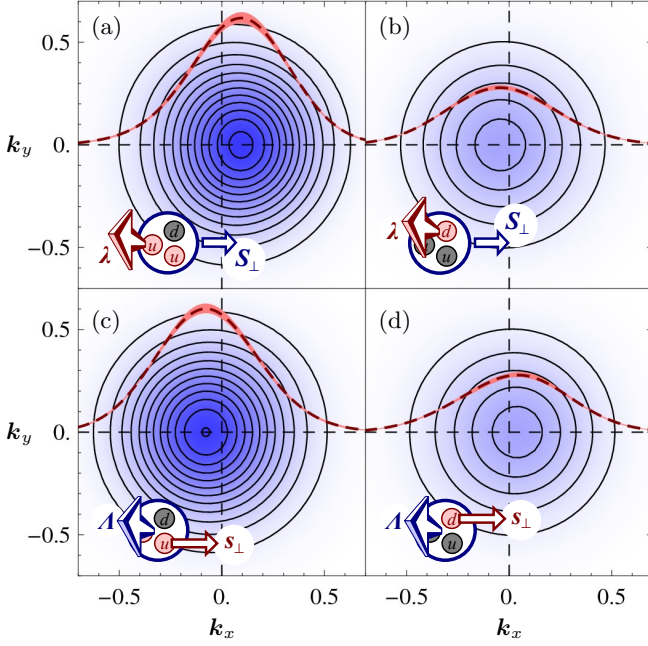


FIG. 3: Quark densities in the  $\mathbf{k}_\perp$ -plane, for  $m_\pi \approx 500$  MeV. (a)  $\rho_L$  for  $u$ -quarks and  $\lambda = 1$ ,  $\mathbf{S}_\perp = (1, 0)$ , (b) the same for  $d$ -quarks, (c)  $\rho_T$  for  $u$ -quarks and  $\Lambda = 1$ ,  $\mathbf{s}_\perp = (1, 0)$ , (d) the same for  $d$ -quarks. The error bands show the density profile at  $\mathbf{k}_y = 0$  as a function of  $\mathbf{k}_x$  (scale not shown).

and Boer-Mulders functions are absent for straight Wilson lines. We stress that the dipole-correlations of the types  $\propto \lambda \mathbf{k}_\perp \cdot \mathbf{S}_\perp g_{1T}$  and  $\propto \Lambda \mathbf{k}_\perp \cdot \mathbf{s}_\perp h_{1L}^\perp$  in Eqs. 4 are a characteristic feature of intrinsic transverse momentum, and that analogous terms in the case of spatial (impact parameter) densities are forbidden by time reversal symmetry [9]. Based on our results for the  $\mathbf{k}_\perp$ -distributions, we show in the upper part of Fig. 3 the lowest  $x$ -moment of the  $\mathbf{k}_\perp$ -density  $\rho_L$  of longitudinally polarized  $u$ - and  $d$ -quarks in a transversely polarized nucleon, with  $\lambda = +1$  and  $\mathbf{S}_\perp = (1, 0)$ . The densities feature significant dipole deformations along the direction of the nucleon spin  $\mathbf{S}_\perp$ , due to non-vanishing average transverse momentum shifts  $\langle \mathbf{k}_x \rangle = m_N g_{1T}^{(0,1)} / f_1^{(0,0)}$ . We find sizeable shifts of  $\langle \mathbf{k}_x \rangle = 67(5)$  MeV for  $u$ -, and  $\langle \mathbf{k}_x \rangle = -30(5)$  MeV for  $d$ -quarks. An analogous observation is made for transversely polarized quarks in a longitudinally polarized nucleon, as displayed in the lower part of Fig. 3 for  $\Lambda = +1$  and  $\mathbf{s}_\perp = (1, 0)$ . Here we find shifts of similar magnitude but opposite sign:  $\langle \mathbf{k}_x \rangle = m_N h_{1L}^{\perp(0,1)} / f_1^{(0,0)} = -60(5)$  MeV for  $u$ -, and  $\langle \mathbf{k}_x \rangle = 16(5)$  MeV for  $d$ -quarks. We note that these intrinsic  $\mathbf{k}_\perp$ -shifts are orthogonal to the dipole deformations  $\propto \mathbf{s}_j \epsilon_{ji} \mathbf{b}_i$  of densities in impact parameter space observed in [10].

**Conclusions.**— We studied tmdPDFs of the nucleon for the first time using lattice QCD. We found that the  $x$  and the  $\mathbf{k}_\perp$  dependence approximately factorizes and that quarks in the nucleon carry significant intrinsic

transverse momentum. The  $\mathbf{k}_\perp$ -densities for polarized quarks in a polarized nucleon show characteristic dipole deformations along the transverse spin vectors. This work represents a first milestone in the non-perturbative calculation of  $\mathbf{k}_\perp$ -distributions. Ongoing studies including non-straight Wilson lines promise in particular to give access to the highly interesting T-odd Sivers effect.

The authors acknowledge support by the Emmy-Noether program and the cluster of excellence “Origin and Structure of the Universe” of the DFG (Ph.H. and B.M.), SFB/TRR-55 (A.S.) and the US Department of Energy grant DE-FG02-94ER40818 (J.N.).

\* Electronic address: [phaegler@ph.tum.de](mailto:phaegler@ph.tum.de)

- [1] R. N. Cahn, Phys. Lett. **B78**, 269 (1978).
- [2] S. J. Brodsky, D. S. Hwang, and I. Schmidt, Phys. Lett. **B530**, 99 (2002); A. V. Belitsky, X. Ji, and F. Yuan, Nucl. Phys. **B656**, 165 (2003).
- [3] D. W. Sivers, Phys. Rev. **D41**, 83 (1990).
- [4] J. C. Collins, Nucl. Phys. **B396**, 161 (1993).
- [5] HERMES Coll. (2009), 0906.3918; M. Alekseev et al. (COMPASS), Phys. Lett. **B673**, 127 (2009); H. Avakian et al. (CLAS), AIP Conf. Proc. **792**, 945 (2005).
- [6] X.-d. Ji, J.-p. Ma, and F. Yuan, Phys. Rev. **D71**, 034005 (2005).
- [7] Issues concerning the integrability related to the high- $\mathbf{k}_\perp$  behaviour of tmdPDFs are discussed in, e.g., [27].
- [8] M. Burkardt, Phys. Rev. **D62**, 071503 (2000).
- [9] M. Diehl and P. Hägler, Eur. Phys. J. **C44**, 87 (2005).
- [10] M. Gökeler et al. (QCDSF), Phys. Rev. Lett. **98**, 222001 (2007).
- [11] D. Brömmel et al. (QCDSF), Phys. Rev. Lett. **101**, 122001 (2008).
- [12] P. J. Mulders and R. D. Tangerman, Nucl. Phys. **B461**, 197 (1996); D. Boer and P. J. Mulders, Phys. Rev. **D57**, 5780 (1998).
- [13] M. Burkardt, Phys. Rev. **D66**, 114005 (2002).
- [14] S. Meissner, A. Metz, and K. Goeke, Phys. Rev. **D76**, 034002 (2007).
- [15] J. Collins, PoS **LC2008**, 028 (2008), 0808.2665.
- [16] M. Anselmino et al., Phys. Rev. **D71**, 074006 (2005).
- [17] B. U. Musch, Phd thesis, TUM (2009), 0907.2381.
- [18] B. Musch, Ph. Hägler, A. Schäfer and J.W. Negele, tbp.
- [19] H. Dorn, Fortsch. Phys. **34**, 11 (1986).
- [20] L. Maiani, G. Martinelli, and C. T. Sachrajda, Nucl. Phys. **B368**, 281 (1992); G. Martinelli and C. T. Sachrajda, Phys. Lett. **B354**, 423 (1995), hep-ph/9502352.
- [21] M. Cheng et al., Phys. Rev. **D77**, 014511 (2008); A. Bazavov et al. (2009), 0903.4379.
- [22] C. W. Bernard et al., Phys. Rev. **D64**, 054506 (2001).
- [23] P. Hägler et al. (LHPC), Phys. Rev. **D77**, 094502 (2008).
- [24] R. G. Edwards and B. Joo (SciDAC), Nucl. Phys. Proc. Suppl. **140**, 832 (2005), hep-lat/0409003.
- [25] R. G. Edwards et al. (LHPC), Phys. Rev. Lett. **96**, 052001 (2006).
- [26] R. Jakob, P. J. Mulders, and J. Rodrigues, Nucl. Phys. **A626**, 937 (1997); B. Pasquini, S. Cazzaniga, and S. Boffi, Phys. Rev. **D78**, 034025 (2008).
- [27] A. Bacchetta et al., JHEP **08**, 023 (2008).